Acta Oceanol. Sin., 2020, Vol. 39, No. 5, P. 11–25
https://doi.org/10.1007/s13131-020-1595-z
http://www.hyxb.org.cn
E-mail: hyxbe@263.net

Using a skillful statistical model to predict September sea ice covering Arctic shipping routes

Sha Li[1], Muyin Wang[2, 3], Wenyu Huang[1], Shiming Xu[1], Bin Wang[1, 4], Yuqi Bai[1]*

[1] Ministry of Education Key Laboratory for Earth System Modeling, Department of Earth System Science, Tsinghua University, Beijing 100084, China

[2] Joint Institute for the Study of the Atmosphere and Ocean, University of Washington, Seattle WA, 98195, USA

[3] Pacific Marine Environmental Laboratory, National Oceanic and Atmospheric Administration, Seattle WA, 98115, USA

[4] State Key Laboratory of Numerical Modeling for Atmospheric Sciences and Geophysical Fluid Dynamics (LASG), Institute of Atmospheric Physics, Chinese Academy of Sciences, Beijing 100029, China

Received 2 August 2019; accepted 25 December 2019

Abstract

The rapid decrease in Arctic sea ice cover and thickness not only has a linkage with extreme weather in the mid-latitudes but also brings more opportunities for Arctic shipping routes and polar resource exploration, both of which motivate us to further understand causes of sea-ice variations and to obtain more accurate estimates of sea-ice cover in the future. Here, a novel data-driven method, the causal effect networks algorithm, is applied to identify the direct precursors of September sea-ice extent covering the Northern Sea Route and Transpolar Sea Route at different lead times so that statistical models can be constructed for sea-ice prediction. The whole study area was also divided into two parts: the northern region covered by multiyear ice and the southern region covered by seasonal ice. The forecast models of September sea-ice extent in the whole study area (TSIE) and southern region (SSIE) at lead times of 1–4 months can explain over 65% and 79% of the variances, respectively, but the forecast skill of sea-ice extent in the northern region (NSIE) is limited at a lead time of 1 month. At lead times of 1–4 months, local sea-ice concentration and sea-ice thickness have a larger influence on September TSIE and SSIE than other teleconnection factors. When the lead time is more than 4 months, the surface meridional wind anomaly from northern Europe in the preceding autumn or early winter is dominant for September TSIE variations but is comparable to thermodynamic factors for NSIE and SSIE. We suggest that this study provides a complementary approach for predicting regional sea ice and is helpful in evaluating and improving climate models.

Key words: regional sea ice, Arctic shipping routes, machine learning, statistical model, predictions

Citation: Li Sha, Wang Muyin, Huang Wenyu, Xu Shiming, Wang Bin, Bai Yuqi. 2020. Using a skillful statistical model to predict September sea ice covering Arctic shipping routes. Acta Oceanologica Sinica, 39(5): 11–25, doi: 10.1007/s13131-020-1595-z

1 Introduction

The Barents Sea and Kara Sea are both shallow shelf seas covered by a small amount of ice in summer (Loeng, 1991) or nearly ice-free. The variations in ice-free area have a fundamental influence on local biodiversity, especially in the marginal ice zone (MIZ) (Hegseth, 1998; Falk-Petersen et al., 2000; Engelsen et al., 2002; Tamelander et al., 2006). The primary production over the Barents Sea has a large interannual variability affected by changes in the ice-edge position (Wassmann et al., 2006). Model experiments showed that there is an upward trend in primary production when regional sea-ice cover significantly decreases in summer (Ellingsen et al., 2008). The fish and other mammals obtain access to the primary production from phytoplankton and zooplankton through food webs and pelagic–benthic coupling (Tamelander et al., 2006), and permanent ice-free conditions in summer are helpful in maintaining these nutrition supplies (Engelsen et al., 2002).

The northward shift in the ice edge not only stimulates the development of fisheries and aquaculture along the coasts of North Europe and Russia but also provides more chances for Arctic shipping routes, including the Northern Sea Route (NSR) along the Siberian coast, Northwest Passage (NWP) and Transpolar Sea Route (TSR) (Humpert and Raspotnik, 2012). The abundant oil/gas, mineral and fishery resources in the Arctic have attracted much attention from more stakeholders. More importantly, the Arctic has a strategic position in economic and military affairs. Arctic shipping routes are the shortest seaborne trade routes linking Asia to Europe and North America relative to traditional shipping routes, such as the Panama Canal and Suez Canal, thereby efficiently reducing the commercial shipping cost (Zhang et al., 2009). Moreover, the Arctic shipping routes can meet the increasing maritime transportation volume that causes congestion in the narrow traditional routes. It is estimated that the recent large loss of Arctic sea ice will increase the potential

Foundation item: The National Key Research and Development Program of China under contract Nos 2016YFF0202705 and 2018YFA0605904; the Joint Institute for the Study of the Atmosphere and Ocean (JISAO) under contract NOAA Cooperative Agreement NA15OAR4320063, contribution No. 2019-1044, and PMEL contribution No. 5052.
*Corresponding author, E-mail: yuqibai@tsinghua.edu.cn

for Arctic shipping by midcentury, even across the central Arctic Ocean (Smith and Stephenson, 2013; Melia et al., 2016), which may break geopolitical limitations along the NSR and NWP.

Sea-ice reduction brings unprecedented opportunities but causes more climate risks with global warming (Yang et al., 2016), such as extreme cold winters in the northeastern US, northwestern and central Europe and even the Far East regions (Liu et al., 2012; Cohen et al., 2014). The ability to capture sea-ice variations in advance on subseasonal to seasonal time scales has pronounced implications for forecasts of fishing seasons, Arctic shipping routes and extreme weather events. Since 2008, Sea Ice Prediction Network (SIPN) has encouraged contributors including citizen scientists to submit their predicted annual pan-Arctic and regional sea-ice extent minimum to Sea Ice Outlook (SIO) managed by SIPN project via an open sea-ice portal (Wayand et al., 2019) which produces an systematic scientific report on Arctic sea-ice projections from dynamical models, statistical models, mixed models and heuristic models in June, July, and August each year (Stroeve et al., 2014) and explores main drivers of September sea-ice changes by model intercomparison. From SIO reports, a lot of coupled ice-ocean models (Zhang et al., 2008; Massonnet et al., 2011; Kauker et al., 2015) and fully coupled ice-ocean-atmosphere models (Chevallier et al., 2013; Metzger et al., 2014; MacLachlan et al., 2015; Borovikov et al., 2019; Bushuk et al., 2017) have been applied to seasonal sea-ice prediction. The seasonal prediction of dynamical models with the same components is affected by different initial conditions (Blanchard-Wrigglesworth et al., 2011; Msadek et al., 2014; Guemas et al., 2016). For instance, studies showed that the same coupled global climate model (NCEP CFSv2), with different initial conditions (initialized atmospheric and oceanic components with NCEP Climate Forecast System Reanalysis (Saha et al., 2010) and used initial sea-ice thickness from Pan-Arctic Ice Ocean Modeling and Assimilation System (PIOMAS) in Collow et al. (2015) rather than nudging sea-ice concentration (Wu and Grumbine, 2014)) could result in large difference in performance. To improve sea-ice predictions, multivariate data assimilation methods have been also utilized to integrate more credible observations into dynamical models (Massonnet et al., 2015; Zhang et al., 2018a; Liu et al., 2019). In addition, linear and non-linear statistical approaches are comparable to dynamical models in predicting the September Arctic sea-ice extent (Drobot et al., 2006; Tivy et al., 2011; Kapsch et al., 2014; Wang et al., 2016; Williams et al., 2016), although their forecast skills are limited due to the lack of observations and the instability of linkages between predictors and predictands (Holland and Stroeve, 2011). Examples of statistical models are: one is provided by Drew Slater, a non-parametric statistical model of Arctic sea-ice extent, based on the probability of daily sea-ice concentration at lead 60-90 days; the other is by Yuan et al. (2016) who used a linear Markov model for sea-ice concentration and found good forecast performance. These results indicate that reliable estimates of sea-ice cover can be obtained through statistical models.

This study introduces a novel data-driven approach, the causal effect networks (CEN) algorithm (Runge et al., 2015), to explore stable and robust precursors of September sea-ice extent covering both the TSR and the NSR to build statistical forecast models. Considering the difference in sea-ice floe size and thickness distribution in different regions (Horvat and Tziperman, 2015; Zhang et al., 2015), we divided the study area into two parts, the southern MIZ (Barents Sea and Kara Sea) covered by seasonal ice and the northern region (part of the central Arctic Ocean) covered by multiyear ice, and compared their precursors. In fact, the CEN method has been employed in many climate research fields, such as the teleconnection among different modes of atmospheric low-frequency variability and between Arctic factors and mid-latitude winter circulation and the prediction of extreme polar vortex events (Ebert-Uphoff and Deng, 2012; Kretschmer et al., 2016, 2017; Li et al., 2018). Compared with other statistical methods, this algorithm has two major advantages: (1) exclusion of false factors due to common drivers or indirect correlations through other variables and (2) identification of the specific lead time and location of each precursor.

2 Materials and methods

2.1 *Data*

According to previous studies on the causes of sea-ice changes, we chose twelve relevant variables in Table 1. Here, the long-term means and linear trends for each calendar month were removed from the sea-ice extent and the twelve variables because we focus on only the month-on-month influence. Monthly detrended data over 1980–2017 were used to keep the stationarity of the time series. Although it was proved that Atlantic water inflow (AWI) has a large impact on Arctic sea-ice variations (Schlichtholz, 2011; Årthun et al., 2012), the AWI index was not included because there are no long-term observations nor reanalysis products that cover the entire study period.

Table 1. Variables associated with September sea-ice extent within the whole study area

Name	Definition	Region
SIC/%	sea-ice concentration	ice-covered ocean north of 30.98°N
SIT/m	sea-ice thickness	ice-covered ocean north of 49°N
SST/K	sea surface temperature	ocean north of 60°N
DLWF/W·m^{-2}	downward surface longwave radiation flux	ocean north of 60°N
DSWF/W·m^{-2}	downward surface shortwave radiation flux	ocean north of 60°N
SSHF/W·m^{-2}	surface sensible heat flux	ocean north of 60°N
SLHF/W·m^{-2}	surface latent heat flux	ocean north of 60°N
SLP/hPa	sea level pressure	north of 60°N
$U_{10\,\mathrm{m}}$/m·s^{-1}	zonal component of wind at 10 m	north of 60°N
$V_{10\,\mathrm{m}}$/m·s^{-1}	meridional component of wind at 10 m	north of 60°N
VT/K·m^3·s^{-1}	net atmosphere heat transport	60°–90°N, 15°–100°E
OHC/J	ocean heat content integrated from 0 to 700 m	North Atlantic (including Arctic Ocean)
OT/J	ocean temperature integrated from 0 to 100 m	North Atlantic (including Arctic Ocean)
NAO	North Atlantic oscillation index	

The daily and monthly gridded sea-ice concentrations (Comiso, 2017) are obtained from National Snow and Ice Data Center (NSIDC). Similar to the way that NSIDC processed data, the daily sea-ice concentration greater than 15% was firstly used to generate daily sea-ice extent, which was averaged over the month into the monthly sea-ice extent. Hereinafter, September sea-ice extent in the whole study area (Fig. 1) is the predicted variable. The sea-ice thickness data set was obtained from Pan-Arctic Ice Ocean Modeling and Assimilation System (PIOMAS) which couples a 12-category thickness and enthalpy distribution (TED) sea-ice model and Parallel Ocean Program (POP) ocean model (Zhang and Rothrock, 2003, 2005).

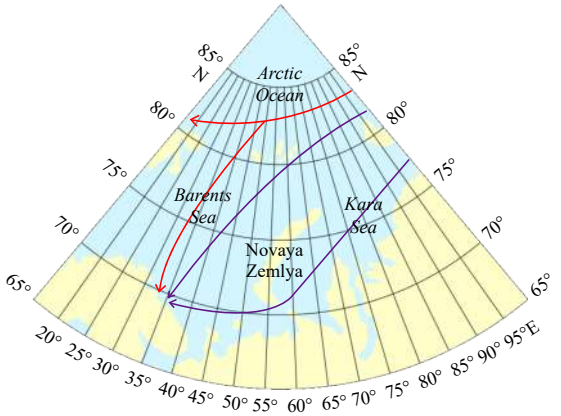

Fig. 1. The whole study area (blue shading) includes the Barents Sea and Kara Sea (65°–81°N, 15°–100°E) and the central Arctic Ocean north of 81°N. Red arrows represent TSR and purple arrows represent NSR.

To investigate the effects of atmospheric and oceanic factors on Arctic sea ice, near-surface fields from ERA-Interim reanalysis (Dee et al., 2011) were used, including sea surface temperature, downward surface longwave and shortwave radiation fluxes, sensible and latent heat fluxes at the surface, sea level pressure, and zonal and meridional components of wind at 10-m height. The net atmosphere heat transport was calculated through the integral of the product of meridional wind and air temperature vertically from 1 000 hPa to 700 hPa in the study area. Ocean heat content and vertically averaged ocean temperature anomaly data are available from Global Ocean Heat and Salt Content database (Levitus et al., 2012). We only used ocean heat content integrated from 0 to 700 m and ocean temperature anomaly integrated from 0 to 100 m, both of which are limited in the North Atlantic basin, including the Arctic Ocean. The monthly North Atlantic Oscillation (NAO) index (Wallace and Gutzler, 1981) was obtained from Climate Prediction Center (CPC)/National Oceanic and Atmospheric Administration (NOAA).

2.2 *Methodology*

2.2.1 *Causal effect networks algorithm*

Similar to Li et al. (2018), lagged correlation fields were first constructed for each relevant variable at lead times of 1–11 months (Figs S1–S7) because this study focuses on the influence of different factors on September TSIE within one year. The statistically significant regions that consist of a broad range of adjacent grids with the same sign on the correlation fields were recognized, and the regional variables were weighted by the correlation coefficients at each grid. Note that several variables (DSWF, SSHF, and SLHF) have no significant-correlative regions. Then, based on the CEN method (Runge et al., 2015), these correlation-weighted regional mean factors and other potential variables (VT, OHC, OT, and NAO) were investigated to determine the direct precursors related to September TSIE through different combinations of minimal and maximal lead times ($1 \leqslant T_{\min} \leqslant T_{\max} \leqslant 11$). The essence of the CEN algorithm is to iteratively test the conditional independence of each factor. That is, given any conditions, partial correlation coefficients of September TSIE with each candidate factor are generated. With the increase in factors as prescribed conditions, the candidate factor was excluded once when any partial correlation coefficient was nonsignificant at the 95% confidence level, which means no robust direct correlation between September TSIE and the candidate factor exists or they have indirect links through some prescribed conditions. Finally, those significant factors directly correlated with September TSIE were retained as predictors in multiple linear regression models.

2.2.2 *Forecast skill scores*

In light of the approach adopted by Lindsay et al. (2008), any consecutive 30 years over 1980–2017 were selected as the fitting period followed by the subsequent two years as the forecast period. Until the 1987–2016 subset, 2017 was the only forecast period. Therefore, 15 values of September TSIE in total were estimated based on the same CEN precursors of regression models at different lead times, and the error variance in these forecasts was

$$\sigma_{\mathrm{f}}^2 = \sum_{i}^{N_{\mathrm{f}}} \left(Y_i - \hat{Y}_i\right)^2 / N_{\mathrm{f}}, \quad N_{\mathrm{f}} = 15, \tag{1}$$

where Y_i and $\hat{Y}_i$ represent the observed and predicted values of the ith forecast sample, respectively. To evaluate the forecast performance, the explained variance in the forecast model relative to climatology was computed by

$$S_{\mathrm{c}}^2 = 1 - \sigma_{\mathrm{f}}^2 / \sigma_{\mathrm{c}}^2. \tag{2}$$

where ${\sigma_{\mathrm{c}}}^2$ was the total variance relative to climatology:

$$\sigma_{\mathrm{c}}^2 = \sum_{j}^{nt} \left(Y_j - \bar{Y}\right)^2 / nt, \quad nt = 38, \tag{3}$$

where Y_j is the observation in the jth year and $\bar{Y}$ is the climatological mean over 1980–2017.

Additionally, to evaluate the stability of regression models, Leave-One-Out cross-validation models were rebuilt on predictors for 1- to 11-month-lead models during the training period after one-year data were removed. The September TSIE in the excluded year was estimated based on its corresponding cross-validation model. The error variance in the cross-validation model was

$$\sigma_{\mathrm{e}}^2 = \sum_{j}^{nt} \left(Y_j - \hat{Y}_j\right)^2 / nt, \tag{4}$$

where Y_j and $\hat{Y}_j$ represent the observed and predicted values in the jth year, respectively. Similar to Eq. (2), the explained variance in the cross-validation model was

$$S_e^2 = 1 - \sigma_e^2/\sigma_c^2. \quad (5)$$

2.2.3 *Monte carlo resampling*

To analyze the impacts of predictors on the uncertainty in the predicted September TSIE, the Monte Carlo method was introduced. Before resampling, it was required to confirm the probability distribution of each precursor. For example, sea-ice concentrations ranging from zero to one accord with the typical Beta distribution. Based on the distribution function of each precursor each year, N=1 000 random numbers were generated and taken into regression models for the 1 000 estimates of September TSIE in that year whose standard deviation was

$$SD_j = \sqrt{\frac{1}{N-1}\sum_i^N \left(Y'_{ij} - \bar{Y}_j\right)^2}, \quad j = 1, 2, \ldots, nt, \quad (6)$$

where Y_{ij}' is the random estimate in the jth year for the ith time and $\bar{Y}_j$ is the mean of all random estimates in the jth year. The standard deviation average over 1980–2017 was used to indicate the contribution of the precursor to the predicted September TSIE.

3 Results

3.1 *Precursors*

According to correlation maps of variables with September TSIE at lead times of 1–11 months, forty statistically significant regions were selected (Figs S1–S7), including two SIC regions, nine SIT regions, four SST regions, six DLWF regions, seven SLP regions, four $U_{10\,m}$ regions and eight $V_{10\,m}$ regions. The parameters of the optimal regression models with predictors included at different lead times are summarized in Table 2, where the minimal lead time represents how long the candidate factor is at least earlier than September. We referred to Eq. (2) and chose the model with the largest explained variance as the optimal model at the specific minimal lead time. All predictors in these optimal

Table 2. Parameters of optimal models of September sea-ice extent within the whole study area at lead times of 1–11 months

T_{min} [1)]	Predictor [2)]	Description	Center coordinates	Regression coefficient [3)]
1	sic_1	August regional mean sea-ice concentration in the 1st group of 2 SIC regions	80.82°N, 68.33°E	0.756
	slp_1	August regional mean sea level pressure in the 1st group of 7 SLP regions	76.21°N, 19.51°E	0.186
	sst_3	January regional mean sea surface temperature in the 3rd group of 4 SST regions	74.13°N, 17.81°E	–0.181
2	sic_2	July regional mean sea-ice concentration in the 2nd group of 2 SIC regions	79.46°N, 61.92°E	0.636
	sit_7	February regional mean sea-ice thickness in the 7th group of 9 SIT regions	82.99°N, 54.10°E	0.254
	v10m_1	July regional mean meridional wind at 10 m in the 1st group of 8 $V_{10\,m}$ regions	82.79°N, 108.87°W	0.204
3	sit_3	June regional mean sea-ice thickness in the 3rd group of 9 SIT regions	82.72°N, 59.17°E	0.681
	v10m_6	December regional mean meridional wind at 10 m in the 6th group of 8 $V_{10\,m}$ regions	70.24°N, 36.89°E	–0.295
	v10m_7	December regional mean meridional wind at 10 m in the 7th group of 8 $V_{10\,m}$ regions	82.23°N, 162.58°E	0.235
4	sit_4	May regional mean sea-ice thickness in the 4th group of 9 SIT regions	82.40°N, 60.92°E	0.576
	u10m_3	May regional mean zonal wind at 10 m in the 3rd group of 4 $U_{10\,m}$ regions	62.98°N, 110.08°E	0.276
	v10m_7	October regional mean meridional wind at 10 m in the 7th group of 8 $V_{10\,m}$ regions	82.23°N, 162.58°E	0.235
5	v10m_4	March regional mean meridional wind at 10 m in the 4th group of 8 $V_{10\,m}$ regions	73.60°N, 86.35°W	–0.377
	v10m_3	April regional mean meridional wind at 10 m in the 3rd group of 8 $V_{10\,m}$ regions	77.74°N, 80.28°E	–0.325
	sst_3	January regional mean sea surface temperature in the 3rd group of 4 SST regions	74.13°N, 17.81°E	–0.344
6	v10m_4	March regional mean meridional wind at 10 m in the 4th group of 8 $V_{10\,m}$ regions	73.60°N, 86.35°W	–0.406
	v10m_6	December regional mean meridional wind at 10 m in the 6th group of 8 $V_{10\,m}$ regions	70.24°N, 36.89°E	–0.433
7	sit_7	February regional mean sea-ice thickness in the 7th group of 9 SIT regions	82.99°N, 54.10°E	0.655
8	sit_8	January regional mean sea-ice thickness in the 8th group of 9 SIT regions	82.42°N, 54.40°E	0.595
9	v10m_6	December regional mean meridional wind at 10 m in the 6th group of 8 $V_{10\,m}$ regions	70.24°N, 36.89°E	–0.569
10	v10m_8	October regional mean meridional wind at 10 m in the 8th group of 8 $V_{10\,m}$ regions	79.86°N, 56.64°E	–0.496
11	v10m_8	October regional mean meridional wind at 10 m in the 8th group of 8 $V_{10\,m}$ regions	79.86°N, 56.64°E	–0.496

Note: [1)] T_{min} represents the minimal lead time for each model. [2)] The number after the underline means the group to which each variable belongs. The specific description of each predictor is shown in the third column. [3)] The regression coefficients correspond to normalized regression models.

models significantly correlate with September TSIE (p<0.05).

From Table 2, August sea-ice concentrations sic_1 (centered on 80.82°N, 68.33°E; hereinafter, the geometric center coordinates of each precursor follow in the parentheses) and July sic_2 (79.46°N, 61.92°E) highly correlate with September TSIE (r>0.8), while sea-ice thickness factors near the study area, June sit_3 (82.72°N, 59.17°E) and May sit_4 (82.40°N, 60.92°E), are closely relevant to September TSIE. Apart from these two kinds of local factors associated with sea-ice physical characteristics, meridional winds at 10-meter height ($V_{10\,\mathrm{m}}$) in different regions at different lead times have some impacts on September TSIE. Among all of $V_{10\,\mathrm{m}}$ factors, v10m_6 (70.24°N, 36.89°E) from northern Europe to Barents Sea, v10m_7 (82.23°N, 162.58°E) north of Laptev Sea and v10m_8 (79.86°N, 56.64°E) near the study area in the previous winter months are viewed as important predictors in over-2-month-lead models, but the effect of October v10m_7 (82.23°N, 162.58°E) on September TSIE is opposite to that of other two $V_{10\,\mathrm{m}}$ factors.

3.2 *Model evaluation*

Based on CEN precursors, multiple linear regression models of September TSIE for a lead time of 1–11 months were constructed. To evaluate their fitting performance, root-mean-square errors (RMSEs) of regression models, persistence models and climatology model were compared (Fig. 2a). The persistence model is based on autocorrelations between the preceding and September TSIE. The climatology model is represented by the long-term mean of September TSIE from 1980 to 2017. The results show that the RMSEs of regression models are less than those of the other two models (RMSE < 0.18×10^6 km^2), which means that regression models have good capability to simulate September TSIE over 1980–2017. However, the fitting skill of the climatology model is worse due to higher RMSE than that of the other two models, which indicates that the variability of September TSIE during the entire study period is very large.

The effects of different combinations of CEN precursors on September TSIE were analyzed. Figure 2b indicates explained variances of regression models, cross-validation models and forecast models, which have the same CEN precursors. The forecast models applied any consecutive 30 years as the fitting period and estimated the September TSIE in the subsequent two years, and finally, 15 predicted values were obtained and used to calculate the explained variances of models (S_c^2). Yet the cross-validation models were constructed with one-year data removed and then September TSIE in the removed year was estimated each time. The results show that explained variances of forecast models are more than 65% when the lead time is less than six months, although the model-building R^2 of the regression model over 1980–2017 decreases with increasing lead time. Furthermore, at lead times of 1–4 months, all explained variances in regression models, cross-validation models based on the leave-one-out cross-validation technique and forecast models are above 50%. Except for 2-month-lead models, other forecast models can explain at least 70% of the variance in September TSIE, which indicates that these models have robust and stable forecast skills for September TSIE.

Figure 3 shows that in either regression models or cross-validation models, there are high correlations between observed and predicted September TSIE (r>0.9). Although models at lead times of 3–4 months overestimate September TSIE when the observed values are approximately 1×10^6 km^2, as a whole, observations and forecasts are significantly correlated at the 95% confidence level. In addition, at the same lead time, the predicted results of regression models and cross-validation models are very close, which implies the high stability of models built on CEN precursors.

To clarify that the CEN method is effective to predict September Arctic sea-ice extent further, we applied ±0.5 standard deviation (SD) of observed September Arctic sea-ice extent over 1980–2013 as the limited scope and evaluated the frequency of predicted values in the limited scope over 2014–2018 for our statistical model based on CEN method (hereinafter referred to as CEN model) and some common SIO dynamical and statistical models over 2014–2018. For example, if the frequency is one, it means only one predicted value for a specific model is in the limited scope during the forecast period (2014–2018), and so on. As is shown in Figs S8 and S9, the frequency of predicted values in the limited scope for CEN models at lead time of 2–3 months is five, which means the difference between predicted and observed September Arctic sea-ice extent over 2014–2018 is still less than 0.5 standard deviation regardless of the lead times. Moreover, only one statistical model provided by Slater (SPIE) is comparable to the CEN model. Apart from them, statistical models provided by Walt Meier and Lamont (Yuan et al. 2016) are more stable respectively at lead 2 and 3 months. As a whole, the forecast skills of statistical models are better than those of dy-

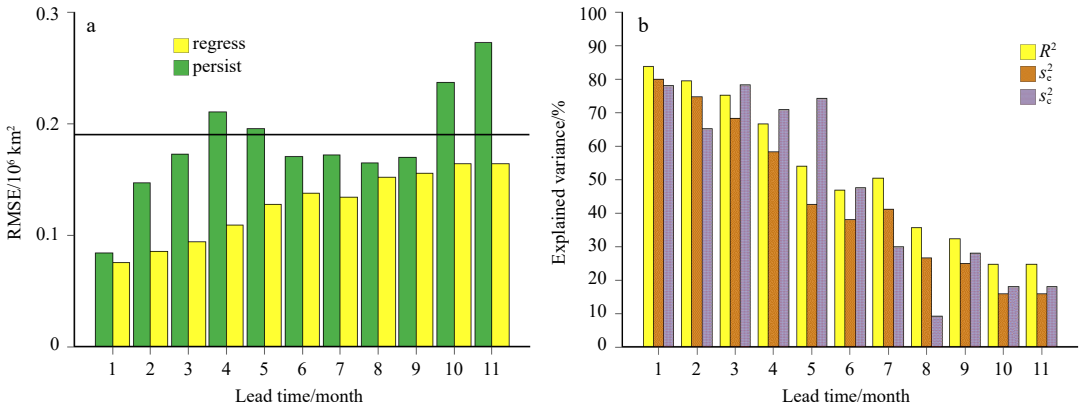

Fig. 2. Fitting and forecast skills of September TSIE models at lead times of 1–11 months. a. Root-mean-square errors. Yellow bars represent regression models, green bars represent persistence models, and black line represents the climatology model. b. Explained variances. Yellow bars represent regression models, orange bars represent cross-validation models, and purple bars represent forecast models.

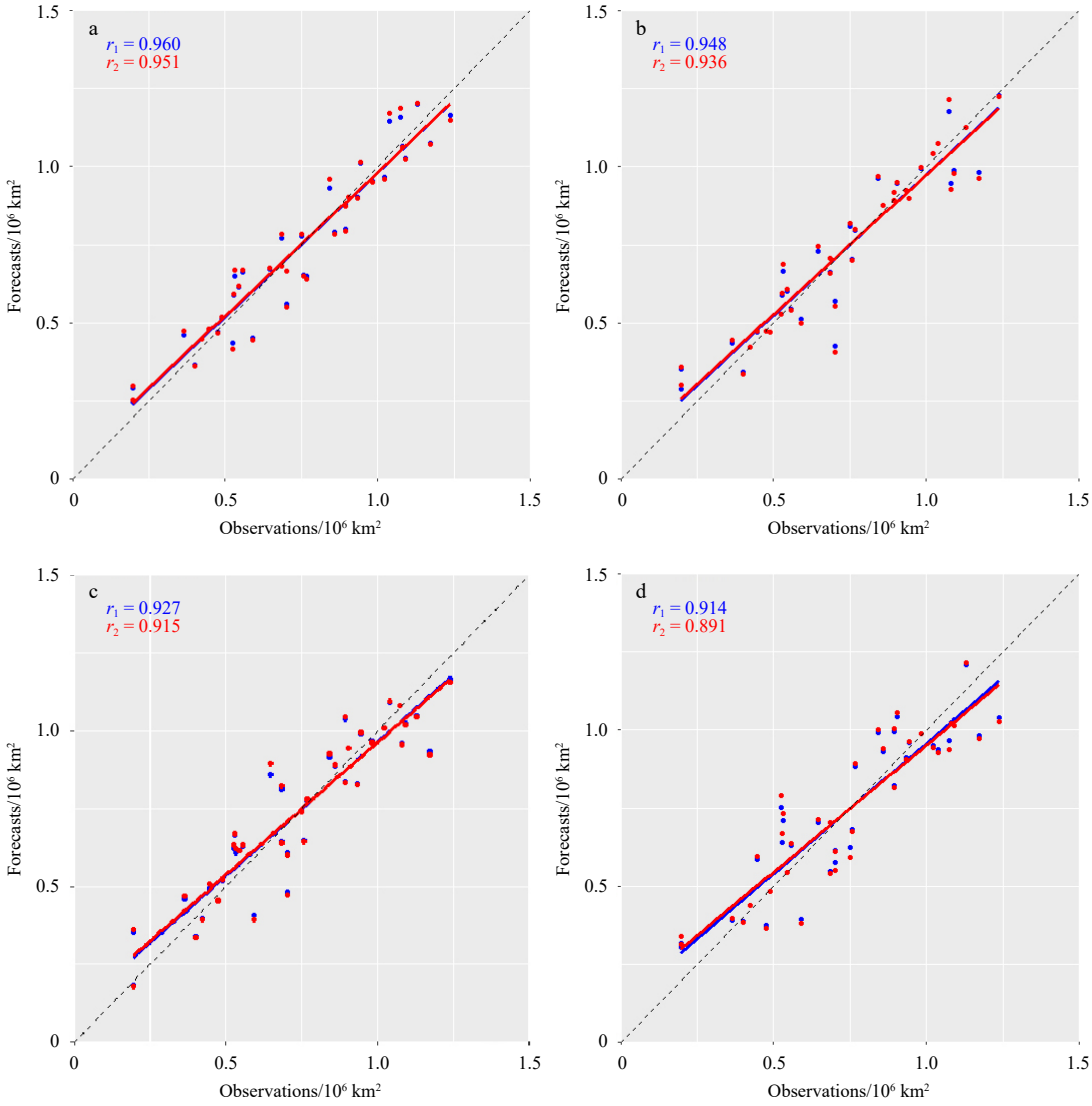

Fig. 3. The observed and predicted September TSIE over 1980–2017. a–d. Results at lead times of 1–4 months respectively. Blue points represent regression models, while red points represent cross-validation models. The blue/red lines indicate linear correlations between observations and forecasts.

namical models. Through comparisons with all of SIO models, the CEN model shows an excellent forecast skill. In contrast to Li et al. (2018), September sea-ice extent in the current study area can be predicted well one month earlier than that in the pan-Arctic region. So we suggest the CEN algorithm is a scientific and competitive prediction method for September sea-ice extent in the pan-Arctic region and other subregions.

3.3 *Uncertainty analysis*

Based on the probability distribution features of different factors, the Monte Carlo resampling technique was applied to all predictors in 1- to 4-month-lead models, where uncertainty ranges caused by predictors with the largest contributions are shown in Fig. 4. These predictors are all local factors related to sea-ice physical characteristics, which result in more than 20% uncertainty in the predicted September TSIE (±0.2×10⁶ km²). Interestingly, sea-ice thickness factors have a larger contribution than sea-ice concentration factors before 2007. Moreover, in the 4-month-lead model, May sit_4 (82.40°N, 60.92°E), sea-ice thickness covering the central Arctic Basin towards the Barents Sea and Kara Sea is the most important precursor to predicted September TSIE, with an average uncertainty contribution of approximately 30% (Fig. 4d).

The impacts of predictors with the second largest contribution on the uncertainty in the predicted September TSIE in 1- to 4-month-lead models are shown in Fig. S10. Except for February sit_7 (82.99°N, 54.10°E) in the 2-month-lead model, external dynamic and thermodynamic factors begin to affect sea-ice changes, but they have much smaller contributions to the uncertainty (below 10%) than those in Fig. 4. It should be emphasized that since 2000, the influence of January sea surface temperature from the east of Greenland to the Barents Sea sst_3 (74.13°N, 17.81°E) is comparable to the local factor of sit_7 (82.99°N, 54.10°E) in February, which indicates that seawater near the North Atlantic can lead to variations in September TSIE by affecting the local sea-ice thickness. Compared with U10m factors in Central Asia in May, v10m_6 (70.24°N, 36.89°E) from northern Europe to the Barents Sea in the preceding December has a

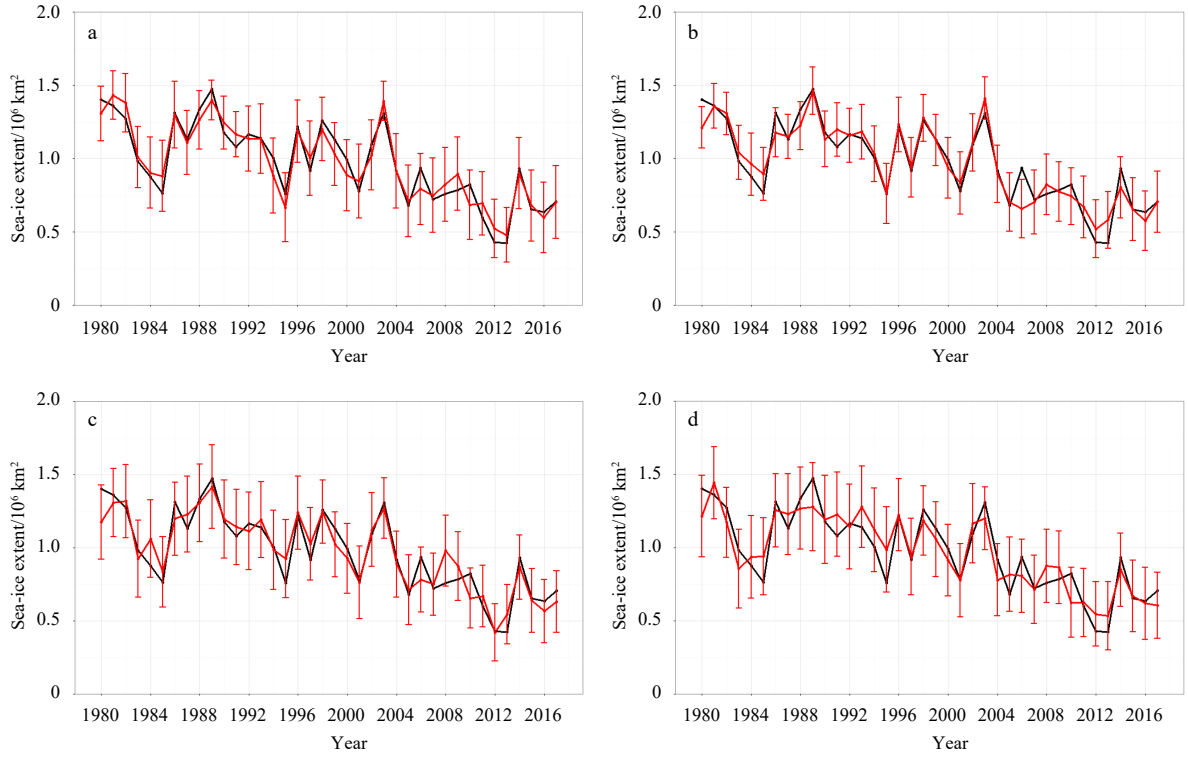

Fig. 4. The uncertainty in the predicted September TSIE caused by major contributors. a. August sic_1, b. July sic_2, c.June sit_3 and d. May sit_4. The black and red lines represent observed and predicted results over 1980–2017 respectively. Red error bars indicate the uncertainty ranges in the predicted results each year.

slightly greater contribution to the uncertainty in the predicted September TSIE. It is likely that the anomalous atmospheric circulation in higher latitudes is helpful for poleward heat transport to accelerate ice melting.

3.4 *Physical explanation*

According to the uncertainty analysis, local factors related to sea-ice physical characteristics play the most prominent roles in 1- to 4-month-lead models, where sea-ice concentration factors at lead times of 1–2 months or sea-ice thickness factors at lead times of 3–4 months have similar effects. From these factors, only two local factors with relatively larger contributions, August sic_1 (80.82°N, 68.33°E) in August and May sit_4 (82.40°N, 60.92°E), were chosen and investigated for their physical relationships with September TSIE. In addition, the impacts of January sst_3 (74.13°N, 17.81°E) and v10m_6 (70.24°N, 36.89°E) in the preceding December on predicted September TSIE were discussed. The locations of these four precursors are shown in Fig. 5.

Figure S11a shows the normalized time series of August sic_1 (80.82°N, 68.33°E) in the northern Barents Sea and Kara Sea from 1980 to 2017. When this precursor is one standard deviation greater than its climatological mean in the positive (negative) phase, it is regarded as the high (low) year. During the period of the late 1980s and mid-1990s, high values of this precursor always appeared, and the precursor was even nearly three standard deviations greater than its climatological mean in 2003. On the other hand, when August sic_1 (80.82°N, 68.33°E) was approximately two standard deviations less than its climatological mean, the extremely low years appeared more than once before the 21st century. In the recent decade, minimal values seldom arose and did not reach an extremely low level.

The causal effect networks algorithm belongs to big data analysis, so it is important to demonstrate how those CEN precursors are linked to September TSIE. Here, a composite analysis was introduced to explore their connections. The composite patterns in Fig. 6 show that in the negative phase of sic_1 (80.82°N, 68.33°E), in the northern Barents and Kara Seas, there exists an extremely negative sea-ice concentration anomaly in August, which leads to the loss of September sea-ice extent in the corresponding region due to its persistence. By contrast, in the positive phase, Arctic sea-ice concentrations obviously increase. It is clear that the local sea-ice concentration factor in August has a direct and pronounced influence on September sea-ice changes in the whole study area.

In Table 2, for a lead time of 3 to 4 months, sea-ice thickness factors become predominant. This study reveals that these precursors related to sea-ice thickness at different lead times almost cover the eastern Arctic, so they can also be viewed as crucial local factors affecting September TSIE. We use May sit_4 (82.40°N, 60.92°E) as an example to unravel the correlation between the previous sea-ice thickness factor and September TSIE in detail. The normalized sit_4 (82.40°N, 60.92°E) in May from 1980 to 2017 is shown in Fig. S11b, where high and low values are marked with red and blue dots, respectively. Similar to that in the August sic_1 (80.82°N, 68.33°E), high years in the May sit_4 (82.40°N, 60.92°E) mainly occurred in the late 1980s and mid-1990s, while low values appeared in the early 1980s, with one rare minimum sea-ice thickness in the recent decade.

When May sit_4 (82.40°N, 60.92°E) is in the negative phase, sea ice covering the north of Canada Archipelago and Greenland and most of the study area is substantially thinner (Fig. 7c), which weakens the internal sea-ice stress so that thinner ice is

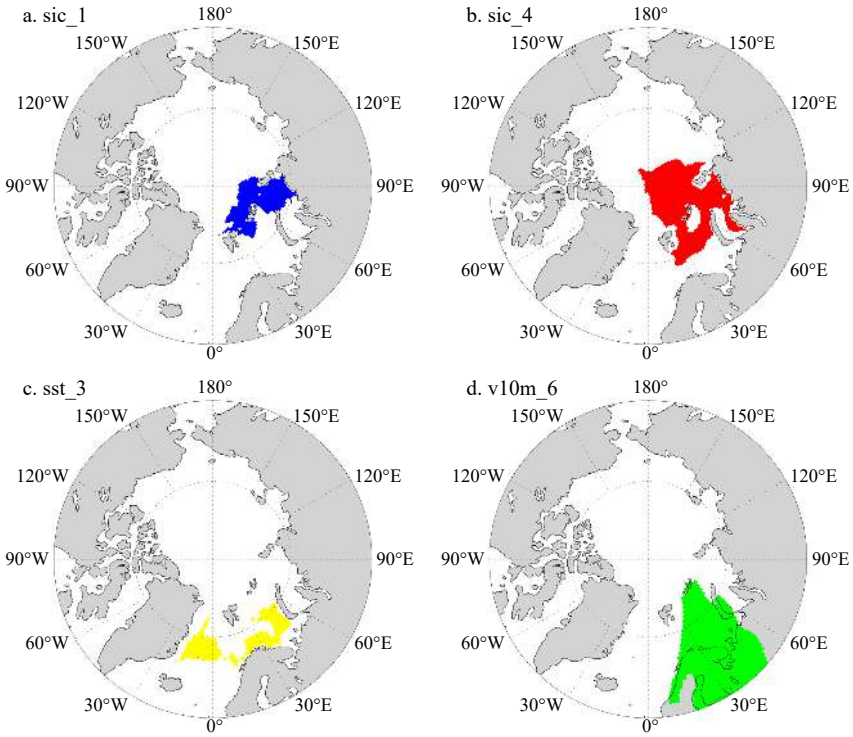

Fig. 5. The spatial distribution of four predictors of September TSIE. a. August sic_1, b. May sit_4, c. January sst_3 and d. December v10m_6.

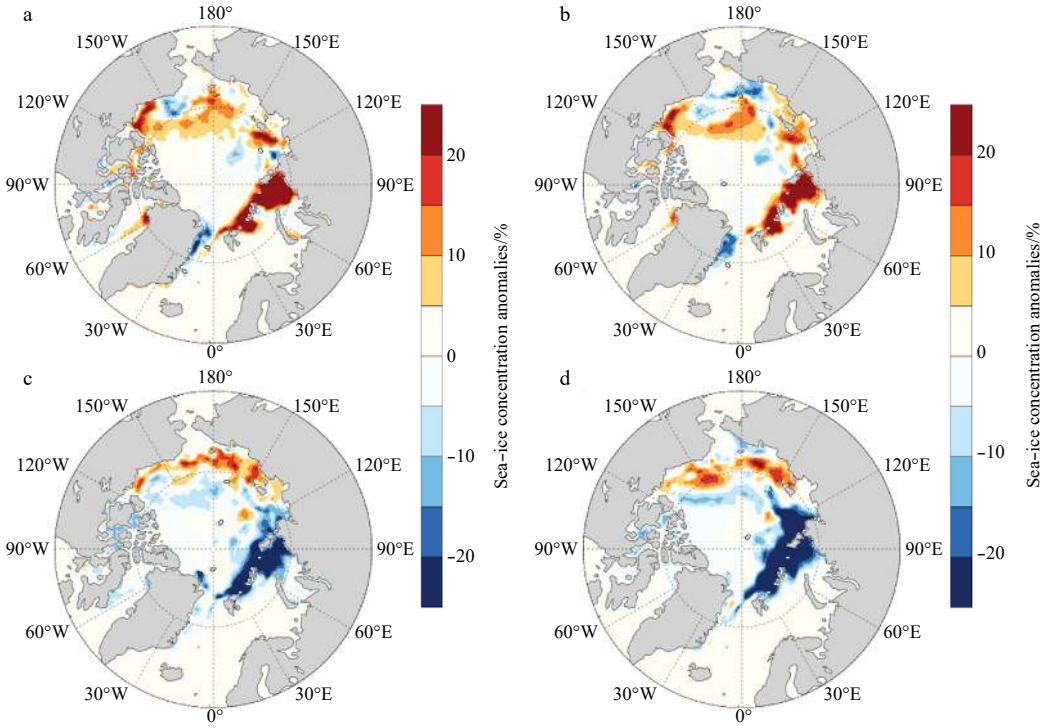

Fig. 6. Composite anomalies of August (a, c) and September (b, d) sea-ice concentrations (shade interval: 5%). The top (bottom) two plots correspond to the years when August sic_1 (80.82°N, 68.33°E) is one standard deviation greater than its climatological mean in the positive (negative) phase.

susceptible to atmospheric and oceanic forcing. This finding has been confirmed in Fig. 7d because the extensive September sea-ice concentration in the corresponding years has a downward trend with sea-ice reduction north of the Barents and Kara Seas most noticeable. The connection between sea-ice thickness in the previous spring and sea-ice concentration in summer is also

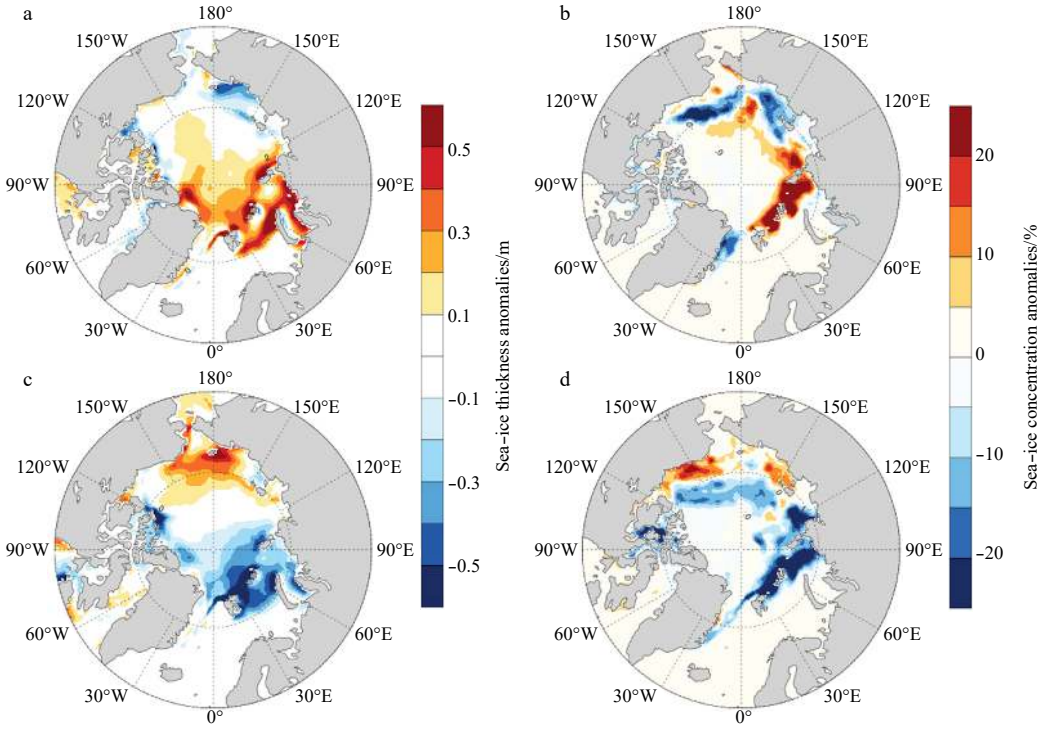

Fig. 7. Composite anomalies of May sea-ice thickness (shade interval: 0.1 m) (a, c) and September sea-ice concentration (shade interval: 5%) (b, d). The top (bottom) two plots correspond to the years when May sit_4 (82.40°N, 60.92°E) is one standard deviation greater than its climatological mean in the positive (negative) phase.

captured in the positive phase of May sit_4 (82.40°N, 60.92°E). The positive sea-ice thickness anomaly in the whole study area helps to maintain the thicker ice and make sea ice difficult to melt (Figs 7a, b). Tilling et al. (2015) also found that the increase of sea-ice thickness northwest of Greenland in Spring led to the restoration of sea-ice cover in autumn 2013 and 2014.

Other than the two local factors related to sea-ice physical characteristics above, January sst_3 (74.13°N, 17.81°E) anti-correlates with September TSIE. Figure S11c reveals that maximal values of the precursor were usually present from the early 1980s and mid-1990s, while minimal values had a dispersed distribution. Since 2005, both high and low years have appeared few times. Nevertheless, to illustrate the connection between January sst_3 (74.13°N, 17.81°E) and September TSIE, composite patterns when this factor is one standard deviation greater than its climatological mean in the positive and/or negative phase were also delineated. During high years of sst_3 (74.13°N, 17.81°E), sea surface temperature east of Greenland and in the Barents Sea is anomalously warm, and this signal lasts for six months until the following summer (Figs 8a–c). It is obvious that the extremely warm regions are located in the entrance where the North Atlantic Current flows into the Arctic, so we suspect that the warm signal of sea surface temperature could be propagated to the Eurasian coast through the flow of seawater (Sakshaug, 1997). This speculation has been corroborated in Fig. 8d because both the strength and the extent of positive sea surface temperature anomaly along the Eurasian coast increase sharply, which is beneficial to sea-ice melting in the study area. In contrast, in the negative phase of January sst_3 (74.13°N, 17.81°E), seawater along the Eurasian coast becomes colder, which impedes sea-ice melting and even accelerates sea-ice growth (Fig. 9). The lagged effect of the North Atlantic Current on Arctic sea ice has been confirmed in other studies using observation measurements (Vinje, 2001) and model experiments (Winton, 2003; Årthun et al., 2012).

Similar to January sst_3 (74.13°N, 17.81°E), v10m_6 (70.24°N, 36.89°E) in the preceding December has a negative correlation with September TSIE. Figure S11c and S11d show that the high and low years of these two precursors are similar, but the variability of regional mean meridional wind at 10-meter height is more striking. In the positive phase of December v10m_6 (70.24°N, 36.89°E), the composite results of meridional wind at 10-meter height and the sea level pressure from the preceding winter to summer are shown in Figs 10a–d, where the low-pressure center east of Greenland in the previous December moves southeastwards with the low-pressure trough intruding into a closed high-pressure system in Central Asia. Until the following September, the high-pressure system shifts to coastal areas of eastern China with a high-pressure ridge northward to the central Arctic Basin, and a closed low-pressure system appears in the vicinity of northern Europe and the Barents Sea. With the development of troughs and ridges, the locations of anomalous sea-ice concentrations vary continually. As shown in Figs 10e–h, sea ice east of Greenland still has a downward trend affected by the concurrent atmospheric circulation (Hilmer et al., 1998). With the low-pressure trough southeastwards, the Barents Sea and Kara Sea are located before the trough and after the ridge in September, so the anomalous southerly wind is helpful in transporting warm air from lower latitudes to the study area causing the large loss of September sea-ice extent (Fig. 10h). Based on the atmospheric data from Atmospheric Infrared Sounder (AIRS), Boisvert et al. (2016) considered that the anomalously warm and wet Barents Sea and Kara Sea region was affected by an Arctic cyclone east of Greenland in December 2015, which in turn increased the re-

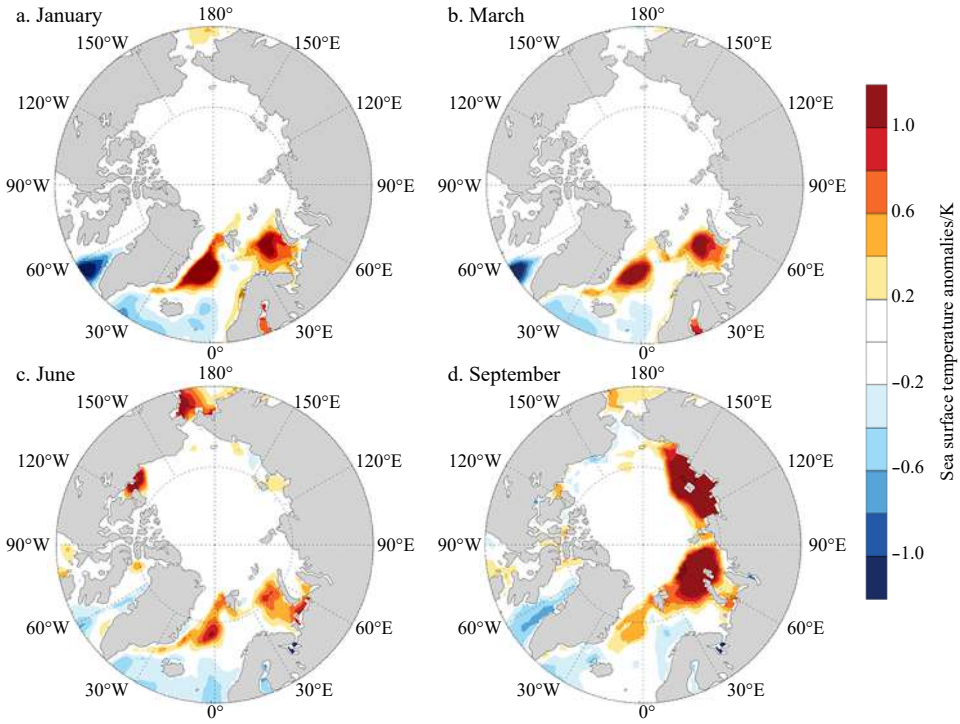

Fig. 8. Composite anomalies of sea surface temperature (shade interval: 0.2 K) when January sst_3 (74.13°N, 17.81°E) is one standard deviation greater than its climatological mean in the positive phase.

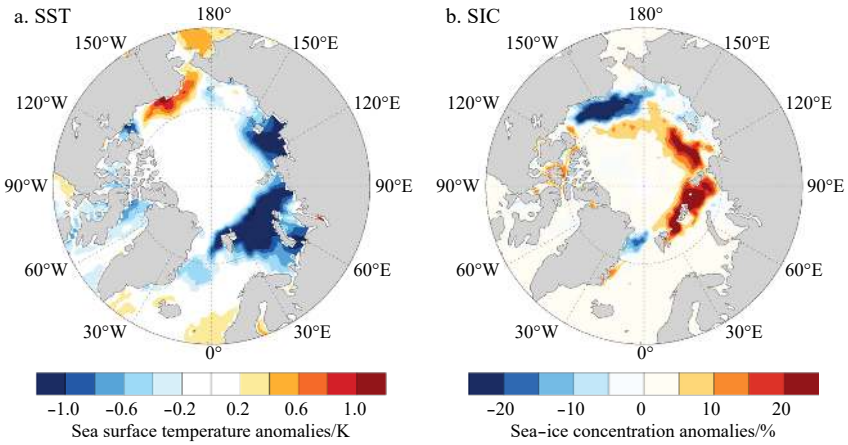

Fig. 9. Composite anomalies of September (a) sea surface temperature (shade interval: 0.2 K) and (b) sea-ice concentration (shade interval: 5%) when January sst_3 (74.13°N, 17.81°E) is one standard deviation greater than its climatological mean in the negative phase.

gional downwelling longwave radiation (Huang et al., 2019) and led to the thinning and loss of sea ice.

4 Discussion

Due to differences in sea-ice structure, the whole study area was also divided into two parts: the southern region (Barents Sea and Kara Sea) covered by thinner seasonal ice and the northern region (central Arctic Ocean) covered by thick multiyear ice. The causal effect networks method was applied to investigate the precursors of September sea-ice extent in these two separate regions. Compared with TSIE, statistical models of September sea-ice extent in the southern region (SSIE) have higher forecast skills with explained variances over 79% (Fig. S12). For SSIE, August sic_1 (79.41°N, 70.40°E) and May sit_4 (81.31°N, 60.79°E) are the same as the corresponding predictors in Figs 5a and b, although the latter have a slightly larger spatial distribution. Another two major predictors of SSIE, July sic_2 (77.75°N, 64.19°E) and June sit_3 (81.81°N, 59.71°E), have similar patterns to those of TSIE. Except for these four major predictors, other predictors of SSIE and TSIE are different at the same amount of lead time, but the proportion of them is much less than that of major predictors in the explained variance in each model at lead times of 1–4 months. For a lead time of more than 4 months, the downward longwave radiation flux (DLWF) anomaly close to the Atlantic Ocean in late winter and spring has a strong positive correlation with September SSIE. When the regional mean DLWF anomaly

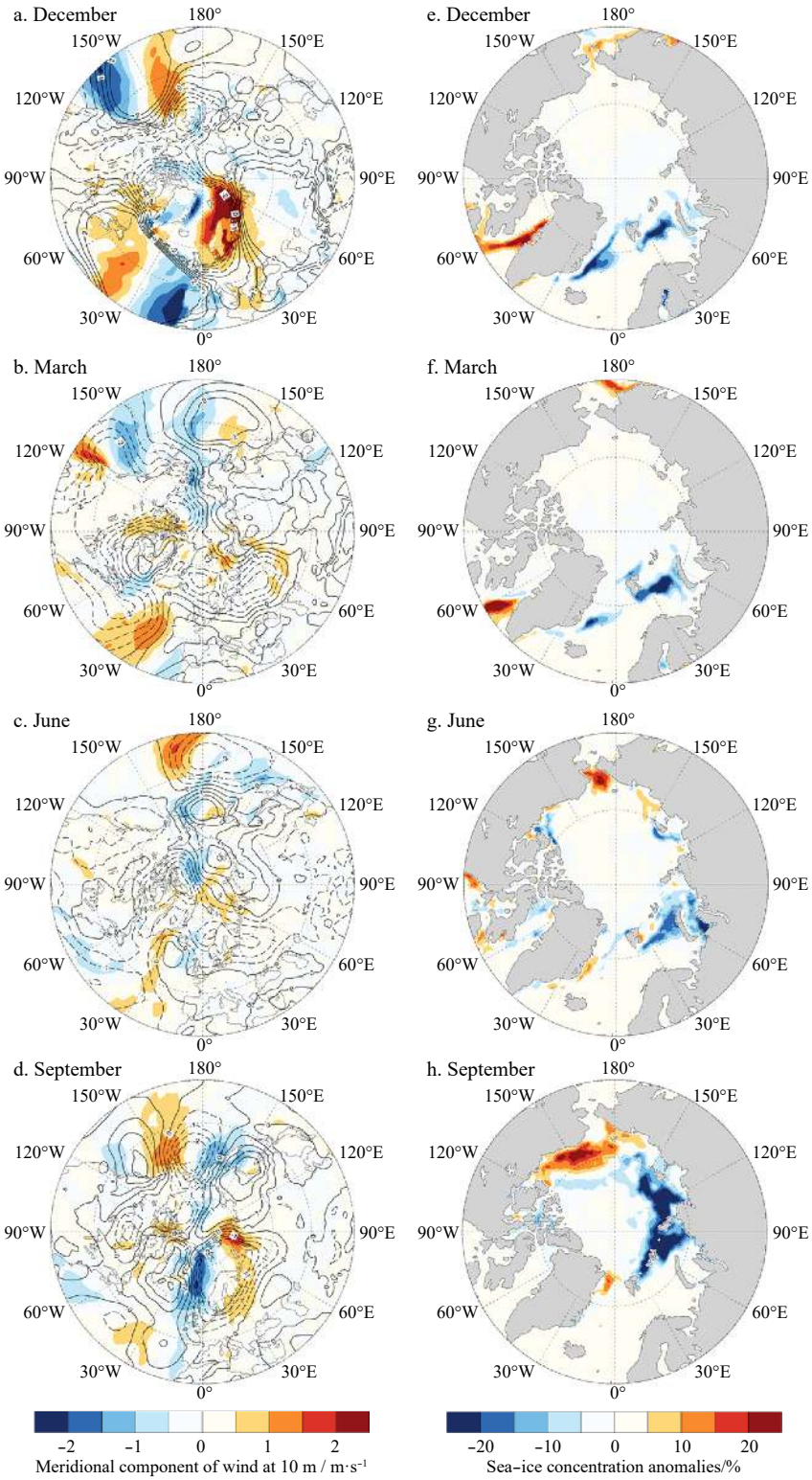

Fig. 10. Composite anomalies of (a–d) meridional component of wind at 10 m (shade interval: 0.5 m/s) and sea level pressure (contour interval: 0.5 hPa) and (e–h) sea-ice concentration (shade interval: 5%) when December v10m_6 (70.24°N, 36.89°E) is one standard deviation greater than its climatological mean in the positive phase. Among the left panels, solid (dashed) contours indicate positive (negative) sea level pressure anomalies.

between Iceland and Norway in January is negative, September SSIE reduces with a positive DLWF anomaly over the Barents Sea and Kara Sea (Fig. S13). Model experiments show that a positive DLWF anomaly in spring motivates earlier ice melt onset, which leads to several radiation feedbacks associated with humidity and cloudiness in the succeeding months and accelerates sea-ice reduction in September (Kapsch et al., 2013, 2016).

Different from SSIE and TSIE, September sea-ice extent in the

northern region (NSIE) can be predicted well at a lead time of 1 month and is mainly affected by October sst_7 (78.49°N, 181.57°E) ranging from the Beaufort Sea to the Laptev Sea, which is comparable to the total contribution of v10 m_7 (66.88°N, 38.28°E) and v10 m_8 (75.43°N, 59.36°E) blowing from northern Europe in the preceding autumn and early winter (Fig. S14) for a lead time of more than two months. As shown in Fig. S15, September NSIE is relatively stable with an extremely low value in 2013, followed by 2012. September Arctic sea-ice cover in 2012 reached a minimum during the whole satellite period, which was directly correlated with a strong storm in August (Zhang et al., 2013). Due to positive ice-albedo feedback, less ice cover led to more open water with increasing solar heating in the upper ocean, which hindered subsequent sea-ice growth (Perovich et al., 2007). The positive sst_7 (78.49°N, 181.57°E) anomaly in October 2012 was captured. Accompanied by anomalous southerly winds, warmer air transported more heat poleward and accelerated sea-ice retreat, which caused a lower NSIE.

Compared with NSIE, September SSIE is much lower during the whole study period (Fig. S15) but has similar major predictors to TSIE, which indicates that the variability of TSIE reflects sea-ice changes over the Barents Sea and Kara Sea rather than those in the central Arctic Ocean. Moreover, it is harder to predict NSIE than SSIE (Koenigk and Mikolajewicz, 2009), which may result from the abrupt decline of NSIE in individual years. Nevertheless, at longer lead times, NSIE and SSIE are both driven by different thermodynamic factors accompanied by southerly wind anomalies, so atmospheric circulation factors exist in all forecast models of September sea-ice extent in different regions.

5 Conclusions

Based on the CEN algorithm, this study investigated the precursors of September TSIE, NSIE and SSIE at lead times of 1–11 months. The results show that 1- to 4-month-lead models have robust and stable forecast performances for TSIE and SSIE, while September NSIE can be well predicted at a lead time of 1 month. In particular, skillful models of TSIE (SSIE) can explain more than 65% (79%) of the variance during forecast periods ($r>0.9$). In all regression models, local sea-ice concentration and sea-ice thickness factors have a larger contribution than other predictors, which reveals that the regional sea-ice variability is mostly governed by local sea-ice conditions. In addition, surface meridional wind and sea surface temperature anomalies in the preceding seasons have a delay effect on September TSIE. For NSIE and SSIE, the role of dynamic and thermodynamic factors is comparable. Sea surface temperature anomalies stemming from the east of Greenland have been proved to significantly correlate with NAO on a decadal time scale (Sandø et al., 2010), but the NAO index was not filtered out. It is likely that the variability of September sea-ice extent does not depend on NAO at a shorter time scale. Likewise, the role of heat content and temperature anomaly in the upper ocean is surpassed by other significant factors that may have been neglected or unrecognized before.

The robust forecast skills of models for September TSIE indicate that if the dominant precursors of regional sea-ice extent are decided, specific models in different subregions can be constructed and estimates of the pan-Arctic sea-ice extent will be more accurate, both of which have far-reaching implications for Arctic shipping routes and extreme climate forecasts. In addition, the teleconnection between precursors and sea-ice extent can be used to identify the source of model biases to improve the forecast skills of dynamical models. Meanwhile, these predictors may provide new insights into the causes of sea-ice variations. On the other hand, some previous studies have found sea-ice cover with different thicknesses, ocean temperature at deeper levels, melt-pond fraction, and sea-ice leads, which can be viewed as important predictors of sea-ice extent (Lindsay et al., 2008; Schröder et al., 2014; Zhang et al., 2018b), so more candidate factors can be used in the causal effect networks algorithm to obtain more detailed physical precursors correlated with sea-ice changes.

Acknowledgements

The causal effect networks algorithm has been developed by Jakob Runge, and the TIGRAMITE software package is available through https://github.com/jakobrunge/tigramite. Thank all of the data development organizations and data websites for datasets available online, including NSIDC, APL/PSC, ECMWF, OCL/NOAA and CPC/NOAA. We are also grateful to Lu Zhou for her help with uncertainty analysis.

References

Årthun M, Eldevik T, Smedsrud L H, et al. 2012. Quantifying the influence of Atlantic heat on Barents Sea ice variability and retreat. Journal of Climate, 25(13): 4736–4743, doi: 10.1175/JCLI-D-11-00466.1

Blanchard-Wrigglesworth E, Bitz C M, Holland M M. 2011. Influence of initial conditions and climate forcing on predicting Arctic sea ice. Geophysical Research Letters, 38(18): L18503

Boisvert L N, Petty A A, Stroeve J C. 2016. The impact of the extreme winter 2015/16 Arctic cyclone on the Barents-Kara Seas. Monthly Weather Review, 144(11): 4279–4287, doi: 10.1175/MWR-D-16-0234.1

Borovikov A, Cullather R, Kovach R, et al. 2019. GEOS-5 seasonal forecast system. Climate Dynamics, 53(12): 7335–7361, doi: 10.1007/s00382-017-3835-2

Bushuk M, Msadek R, Winton M, et al. 2017. Skillful regional prediction of Arctic sea ice on seasonal timescales. Geophysical Research Letters, 44(10): 4953–4964, doi: 10.1002/2017GL073155

Chevallier M, Salasy Mélia D, Voldoire A, et al. 2013. Seasonal forecasts of the pan-Arctic sea ice extent using a GCM-based seasonal prediction system. Journal of Climate, 26(16): 6092–6104, doi: 10.1175/JCLI-D-12-00612.1

Cohen J, Screen J A, Furtado J C, et al. 2014. Recent Arctic amplification and extreme mid-latitude weather. Nature Geoscience, 7(9): 627–637, doi: 10.1038/ngeo2234

Collow T W, Wang Wanqiu, Kumar A, et al. 2015. Improving Arctic sea ice prediction using PIOMAS initial sea ice thickness in a coupled ocean-atmosphere model. Monthly Weather Review, 143(11): 4618–4630, doi: 10.1175/MWR-D-15-0097.1

Comiso J C. 2017. Bootstrap sea ice concentrations from nimbus-7 SMMR and DMSP SSM/I-SSMIS, version 3. [1979–2017] Boulder, Colorado USA: NASA National Snow and Ice Data Center Distributed Active Archive Center, doi: https://doi.org/10.5067/7Q8HCCWS4I0R[2019–02–17]

Dee D P, Uppala S M, Simmons A J, et al. 2011. The ERA-interim reanalysis: configuration and performance of the data assimilation system. Quarterly Journal of the Royal Meteorological Society, 137(656): 553–597, doi: 10.1002/qj.828

Drobot S D, Maslanik J A, Fowler C. 2006. A long-range forecast of Arctic summer sea-ice minimum extent. Geophysical Research Letters, 33(10): L10501

Ebert-Uphoff I, Deng Yi. 2012. Causal discovery for climate research using graphical models. Journal of Climate, 25(17): 5648–5665, doi: 10.1175/JCLI-D-11-00387.1

Ellingsen I H, Dalpadado P, Slagstad D, et al. 2008. Impact of climatic change on the biological production in the Barents Sea. Climatic Change, 87(1–2): 155–175, doi: 10.1007/s10584-007-9369-6

Engelsen O, Hegseth E N, Hop H, et al. 2002. Spatial variability of chlorophyll-a in the Marginal Ice Zone of the Barents Sea, with relations to sea ice and oceanographic conditions. Journal of Marine Systems, 35(1–2): 79–97, doi: 10.1016/S0924-7963(02)00077-5

Falk-Petersen S, Hop H, Budgell W P, et al. 2000. Physical and ecological processes in the marginal ice zone of the northern Barents Sea during the summer melt period. Journal of Marine Systems, 27(1–3): 131–159, doi: 10.1016/S0924-7963(00)00064-6

Guemas V, Chevallier M, Déqué M, et al. 2016. Impact of sea ice initialization on sea ice and atmosphere prediction skill on seasonal timescales. Geophysical Research Letters, 43(8): 3889–3896, doi: 10.1002/2015GL066626

Hegseth E N. 1998. Primary production of the northern Barents Sea. Polar Research, 17(2): 113–123, doi: 10.1111/j.1751-8369.1998.tb00266.x

Hilmer M, Harder M, Lemke P. 1998. Sea ice transport: a highly variable link between Arctic and North Atlantic. Geophysical Research Letters, 25(17): 3359–3362, doi: 10.1029/98GL52360

Holland M M, Stroeve J. 2011. Changing seasonal sea ice predictor relationships in a changing Arctic climate. Geophysical Research Letters, 38(18): L18501

Horvat C, Tziperman E. 2015. A prognostic model of the sea-ice floe size and thickness distribution. The Cryosphere, 9(6): 2119–2134, doi: 10.5194/tc-9-2119-2015

Huang Yi, Chou G, Xie Yan, et al. 2019. Radiative control of the interannual variability of Arctic sea ice. Geophysical Research Letters, 46(16): 9899–9908, doi: 10.1029/2019GL084204

Humpert M, Raspotnik A. 2012. The future of Arctic shipping along the transpolar sea route. In: Heininen L, Exner-Pirot H, Plouffe J, eds. Arctic Yearbook. Akureyri: Northern Research Forum, 281–307

Kapsch M L, Graversen R G, Economou T, et al. 2014. The importance of spring atmospheric conditions for predictions of the Arctic summer sea ice extent. Geophysical Research Letters, 41(14): 5288–5296, doi: 10.1002/2014GL060826

Kapsch M L, Graversen R G, Tjernström M. 2013. Springtime atmospheric energy transport and the control of Arctic summer sea-ice extent. Nature Climate Change, 3(8): 744–748, doi: 10.1038/nclimate1884

Kapsch M L, Graversen R G, Tjernström M, et al. 2016. The effect of downwelling longwave and shortwave radiation on Arctic summer sea ice. Journal of Climate, 29(3): 1143–1159, doi: 10.1175/JCLI-D-15-0238.1

Kauker F, Kaminski T, Ricker R, et al. 2015. Seasonal sea ice predictions for the Arctic based on assimilation of remotely sensed observations. The Cryosphere Discussions, 9(5): 5521–5554, doi: 10.5194/tcd-9-5521-2015

Koenigk T, Mikolajewicz U. 2009. Seasonal to interannual climate predictability in mid and high northern latitudes in a global coupled model. Climate Dynamics, 32(6): 783–798, doi: 10.1007/s00382-008-0419-1

Kretschmer M, Coumou D, Donges J F, et al. 2016. Using causal effect networks to analyze different arctic drivers of midlatitude winter circulation. Journal of Climate, 29(11): 4069–4081, doi: 10.1175/JCLI-D-15-0654.1

Kretschmer M, Runge J, Coumou D. 2017. Early prediction of extreme stratospheric polar vortex states based on causal precursors. Geophysical Research Letters, 44(16): 8592–8600, doi: 10.1002/2017GL074696

Levitus S, Antonov J I, Boyer T P, et al. 2012. World ocean heat content and thermosteric sea level change (0–2 000 m), 1955–2010. Geophysical Research Letters, 39(10): L10603

Li Sha, Wang Muyin, Bond N A, et al. 2018. Precursors of September arctic sea-ice extent based on causal effect networks. Atmosphere, 9(11): 437, doi: 10.3390/atmos9110437

Lindsay R W, Zhang Jinlun, Schweiger A J, et al. 2008. Seasonal predictions of ice extent in the Arctic Ocean. Journal of Geophysical Research, 113(C2): C02023

Liu Jiping, Chen Zhiqiang, Hu Yongyun, et al. 2019. Towards reliable Arctic sea ice prediction using multivariate data assimilation. Science Bulletin, 64(1): 63–72, doi: 10.1016/j.scib.2018.11.018

Liu Jiping, Curry J A, Wang Huijun, et al. 2012. Impact of declining Arctic sea ice on winter snowfall. Proceedings of the National Academy of Sciences of the United States of America, 109(11): 4074–4079, doi: 10.1073/pnas.1114910109

Loeng H. 1991. Features of the physical oceanographic conditions of the Barents Sea. Polar Research, 10(1): 5–18, doi: 10.3402/polar.v10i1.6723

MacLachlan C, Arribas A, Peterson K A, et al. 2015. Global Seasonal forecast system version 5 (GloSea5): a high–resolution seasonal forecast system. Quarterly Journal of the Royal Meteorological Society, 141(689): 1072–1084, doi: 10.1002/qj.2396

Massonnet F, Fichefet T, Goosse H, et al. 2011. On the influence of model physics on simulations of Arctic and Antarctic sea ice. The Cryosphere, 5(3): 687–699, doi: 10.5194/tc-5-687-2011

Massonnet F, Fichefet T, Goosse H. 2015. Prospects for improved seasonal Arctic sea ice predictions from multivariate data assimilation. Ocean Modelling, 88: 16–25, doi: 10.1016/j.ocemod.2014.12.013

Melia N, Haines K, Hawkins E. 2016. Sea ice decline and 21st century trans-Arctic shipping routes. Geophysical Research Letters, 43(18): 9720–9728, doi: 10.1002/2016GL069315

Metzger E J, Smedstad O M, Thoppil P G, et al. 2014. US Navy operational global ocean and Arctic ice prediction systems. Oceanography, 27(3): 32–43, doi: 10.5670/oceanog.2014.66

Msadek R, Vecchi G A, Winton M, et al. 2014. Importance of initial conditions in seasonal predictions of Arctic sea ice extent. Geophysical Research Letters, 41(14): 5208–5215, doi: 10.1002/2014GL060799

Perovich D K, Light B, Eicken H, et al. 2007. Increasing solar heating of the Arctic Ocean and adjacent seas, 1979–2005: attribution and role in the ice-albedo feedback. Geophysical Research Letters, 34(19): L19505, doi: 10.1029/2007GL031480

Runge J, Petoukhov V, Donges J F, et al. 2015. Identifying causal gateways and mediators in complex spatio-temporal systems. Nature Communications, 6: 8502, doi: 10.1038/ncomms9502

Saha S, Moorthi S, Pan Hualu, et al. 2010. The NCEP climate forecast system reanalysis. Bulletin of the American Meteorological Society, 91(8): 1015–1058, doi: 10.1175/2010BAMS3001.1

Sakshaug E. 1997. Biomass and productivity distributions and their variability in the Barents Sea. ICES Journal of Marine Science, 54(3): 341–350, doi: 10.1006/jmsc.1996.0170

Sandø A B, Nilsen J E Ø, Gao Y, et al. 2010. Importance of heat transport and local air–sea heat fluxes for Barents Sea climate variability. Journal of Geophysical Research, 115(C7): C07013

Schlichtholz P. 2011. Influence of oceanic heat variability on sea ice anomalies in the Nordic Seas. Geophysical Research Letters, 38(5): L05705

Schröder D, Feltham D L, Flocco D, et al. 2014. September Arctic sea-ice minimum predicted by spring melt-pond fraction. Nature Climate Change, 4(5): 353–357, doi: 10.1038/nclimate2203

Smith L C, Stephenson S R. 2013. New trans-Arctic shipping routes navigable by midcentury. Proceedings of the National Academy of Sciences of the United States of America, 110(13): E1191–E1195, doi: 10.1073/pnas.1214212110

Stroeve J, Hamilton L C, Bitz C M, et al. 2014. Predicting September sea-ice: ensemble skill of the SEARCH sea ice outlook 2008–2013. Geophysical Research Letters, 41(7): 2411–2418, doi: 10.1002/2014GL059388

Tamelander T, Renaud P E, Hop H, et al. 2006. Trophic relationships and pelagic-benthic coupling during summer in the Barents Sea Marginal Ice Zone, revealed by stable carbon and nitrogen isotope measurements. Marine Ecology Progress Series, 310: 33–46, doi: 10.3354/meps310033

Tilling R L, Ridout A, Shepherd A, et al. 2015. Increased Arctic sea ice volume after anomalously low melting in 2013. Nature Geoscience, 8(8): 643–646, doi: 10.1038/ngeo2489

Tivy A, Howell S E L, Alt B, et al. 2011. Origins and levels of seasonal forecast skill for sea ice in Hudson Bay using canonical correlation analysis. Journal of Climate, 24(5): 1378–1395, doi: 10.1175/2010JCLI3527.1

Vinje T. 2001. Anomalies and trends of sea-ice extent and atmospheric circulation in the Nordic seas during the period 1864–1998. Journal of Climate, 14(3): 255–267, doi: 10.1175/1520-0442(2001)014<0255:AATOSI>2.0.CO;2

Wallace J M, Gutzler D S. 1981. Teleconnections in the geopotential

height field during the Northern Hemisphere winter. Monthly Weather Review, 109(4): 784–812, doi: 10.1175/1520-0493(1981)109<0784:TITGHF>2.0.CO;2

Wang Lei, Yuan Xiaojun, Ting Mingfang, et al. 2016. Predicting summer arctic sea ice concentration intraseasonal variability using a vector autoregressive model. Journal of Climate, 29(4): 1529–1543, doi: 10.1175/JCLI-D-15-0313.1

Wassmann P, Reigstad M, Haug T, et al. 2006. Food webs and carbon flux in the Barents Sea. Progress in Oceanography, 71(2–4): 232–287, doi: 10.1016/j.pocean.2006.10.003

Wayand N E, Bitz C M, Blanchard-Wrigglesworth E. 2019. A year-round subseasonal-to-seasonal sea ice prediction portal. Geophysical Research Letters, 46(6): 3298–3307, doi: 10.1029/2018GL081565

Williams J, Tremblay B, Newton R, et al. 2016. Dynamic preconditioning of the minimum September sea-ice extent. Journal of Climate, 29(16): 5879–5891, doi: 10.1175/JCLI-D-15-0515.1

Winton M. 2003. On the climatic impact of ocean circulation. Journal of Climate, 16(17): 2875–2889, doi: 10.1175/1520-0442(2003)016<2875:OTCIOO>2.0.CO;2

Wu Xingren, Grumbine R. 2014. Sea Ice in the NCEP Climate Forecast System. Climate Prediction S&T Digest. Science and Technology Infusion Climate Bulletin Supplement February 2014, 28–35

Yang Shili, Dong Wenjie, Chou Jieming, et al. 2016. Global warming projections using the human-earth system model BNU-HESM1.0. Science Bulletin, 61(23): 1833–1838, doi: 10.1007/s11434-016-1176-x

Yuan Xiaojun, Chen Dake, Li Cuihua, et al. 2016. Arctic sea ice seasonal prediction by a linear Markov model. Journal of Climate, 29(22): 8151–8173, doi: 10.1175/JCLI-D-15-0858.1

Zhang Yongfei, Bitz C M, Anderson J L, et al. 2018a. Insights on sea ice data assimilation from perfect model observing system simulation experiments. Journal of Climate, 31(15): 5911–5926, doi: 10.1175/JCLI-D-17-0904.1

Zhang Yuanyuan, Cheng Xiao, Liu Jiping, et al. 2018b. The potential of sea ice leads as a predictor for summer Arctic sea ice extent. The Cryosphere, 12(12): 3747–3757, doi: 10.5194/tc-12-3747-2018

Zhang Jinlun, Lindsay R, Schweiger A, et al. 2013. The impact of an intense summer cyclone on 2012 Arctic sea ice retreat. Geophysical Research Letters, 40(4): 720–726, doi: 10.1002/grl.50190

Zhang Jinlun, Rothrock D A. 2003. Modeling global sea ice with a thickness and enthalpy distribution model in generalized curvilinear coordinates. Monthly Weather Review, 131(5): 845–861, doi: 10.1175/1520-0493(2003)131<0845:MGSIWA>2.0.CO;2

Zhang Jinlun, Rothrock D A. 2005. Effect of sea ice rheology in numerical investigations of climate. Journal of Geophysical Research, 110(C8): C08014

Zhang Jinlun, Schweiger A, Steele M, et al. 2015. Sea ice floe size distribution in the marginal ice zone: theory and numerical experiments. Journal of Geophysical Research, 120(5): 3484–3498

Zhang Jinlun, Steele M, Lindsay A, et al. 2008. Ensemble 1-Year predictions of arctic sea ice for the spring and summer of 2008. Geophysical Research Letters, 35(8): L08502

Zhang Xia, Tu Jingfang, Guo Peiqing, et al. 2009. The economic estimate of arctic sea routes and its strategic significance for the development of Chinese economy. China Soft Science (in Chinese), (S2): 86–93

Supplementary information:

Fig. S1. Correlation maps of sea-ice concentration with September sea-ice extent over 65°–90°N, 15°–100°E (TSIE) at lead times of 1–11 months. The red and blue colors represent positive and negative correlations respectively. Raster shadings indicate the significantly correlative regions at the 95% (p<0.05) confidence level.

Fig. S2. Correlation maps of sea-ice thickness with September TSIE at lead times of 1–11 months. The red and blue colors represent positive and negative correlations respectively. Raster shadings indicate the significantly correlative regions at the 95% (p<0.05) confidence level.

Fig. S3. Correlation maps of sea surface temperature with September TSIE at lead times of 1–11 months. The red and blue colors represent positive and negative correlations respectively. Raster shadings indicate the significantly correlative regions at the 95% (p<0.05) confidence level.

Fig. S4. Correlation maps of downward surface longwave radiation flux with September TSIE at lead times of 1–11 months. The red and blue colors represent positive and negative correlations respectively. Raster shadings indicate the significantly correlative regions at the 95% (p<0.05) confidence level.

Fig. S5. Correlation maps of sea level pressure with September TSIE at lead times of 1–11 months. The red and blue colors represent positive and negative correlations respectively. Raster shadings indicate the significantly correlative regions at the 95% (p<0.05) confidence level.

Fig. S6. Correlation maps of zonal component of wind at 10 m height with September TSIE at lead times of 1–11 months. The red and blue colors represent positive and negative correlations respectively. Raster shadings indicate the significantly correlative regions at the 95% (p<0.05) confidence level.

Fig. S7. Correlation maps of meridional component of wind at 10 m height with September TSIE at lead times of 1–11 months. The red and blue colors represent positive and negative correlations respectively. Raster shadings indicate the significantly correlative regions at the 95% (p<0.05) confidence level.

Fig. S8. Frequency of predicted September Arctic sea-ice extent in the limited scope (±0.5 SD) over 2014–2018 for CEN model (blue), SIO statistical models (brown) and dynamical models (yellow) at lead 2 months. *Y* Axis labels represent model contributors.

Fig. S9. Frequency of predicted September Arctic sea-ice extent in the limited scope (±0.5 SD) over 2014–2018 for CEN model (blue), SIO statistical models (brown) and dynamical models (yellow) at lead 3 months. *Y* Axis labels represent model contributors.

Fig. S10. The uncertainty in the predicted September TSIE caused by January sst_3 (a) , February sit_7 (b), December v10m_6 (c) and May u10m_3 (d). The black and red lines represent observed and predicted results over 1980–2017 respectively. Red error bars represent the uncertainty ranges in the predicted results each year.

Fig. S11. Normalized time series of four predictors of September TSIE over 1980-2017. a. August sic_1 (80.82°N, 68.33°E), b. May sit_4 (82.40°N, 60.92°E), c. January sst_3 (74.13°N, 17.81°E), and d. December v10m_6 (70.24°N, 36.89°E) . Red (blue) dots correspond to the years when one predictor is one standard deviation (1 SD) greater than its climatological mean in the positive (negative) phase. Black dots correspond to the years when one predictor is one standard deviation less than its climatological mean in the positive or negative phase. Dashed lines represent ±1 SD.

Fig. S12. Explained variances of September SSIE models at lead times of 1-11 months. Yellow bars represent regression models, orange bars represent cross-validation models, and pink bars represent forecast models.

Fig. S13. Composite anomalies of downward surface longwave radiation flux (shade interval: 2 W/m^2) when January dlwf_5 (64.06°N, 7°W) is one standard deviation greater than its climatological mean in the negative phase.

Fig. S14. The spatial distribution of October sst_7 (a) , December v10m_7 (b) , and October v10m_8 (c). These factors are main predictors of September NSIE for the lead time of more than 2 months.

Fig. S15. Time series of September sea-ice extent in the whole study area (blue line), northern region (yellow line), and southern region (gray line).

The supplementary information is available online at https://doi.org/10.1007/s13131-020-1595-z. The supplementary information is published as submitted, without typesetting or editing. The responsibility for scientific accuracy and content remains entirely with the authors.